Density and H_α diagnostics and results for the sustained spheromak physics experiment

Zhehui Wang,[a] G. A. Wurden, Cris W. Barnes, and C. J. Buchenauer
Los Alamos National Laboratory, Los Alamos, New Mexico 87545

H. S. McLean, D. N. Hill, E. B. Hooper, R. D. Wood, and S. Woodruff
Lawrence Livermore National Laboratory, Livermore, California 94550

(Presented on 21 June 2000)

A newly installed density diagnostic using CO_2 laser interferometry and an H_α diagnostic using interference filters and photomultiplier tubes for the recently constructed sustained spheromak physics experiment (SSPX) are described. First diagnostic results of the H_α diagnostic were useful to understand the breakdown physics in the new SSPX experiments. Low-noise density data validates techniques to reduce vibration and electronic pickup. The data-processing electronics of the new interferometer can yield unambiguous density data that is equivalent to 16 fringe shifts. Density data is also critical to understand the particle source, and the J/n_e parameter for SSPX. © *2001 American Institute of Physics.* [DOI: 10.1063/1.1319364]

I. INTRODUCTION

Spheromaks are compact toroids where the internal plasma current generates most of the magnetic field. It was predicted that through ohmic heating (ηJ^2) alone, fusion breakeven condition may be achieved in spheromaks.[1,2] The sustained spheromak physics experiment (SSPX)[3] was designed to achieve electron and ion temperatures of a few hundred electron volts in steady-state spheromaks driven by direct current (dc) magnetic helicity injection. To reach this goal, radiation due to impurities and Bremsstralung electrons needs to be minimized. The power balance for electrons in a radiation-dominated plasma can be approximated by the equation $\eta J^2 = n_e^2 R(T_e)$, where $R(T_e)$ is the functional dependence of the radiation on the electron temperature. Therefore, the J/n_e parameter essentially determines the electron temperature. A reasonably hot spheromak usually would have its J/n_e ratio exceeding 2×10^{-14} A m.

Plasma density control is an important aspect of the J/n_e maximization. A density measurement is critical for the development of density control techniques. A 10.6 μm multichord CO_2 laser interferometer was used for the density and J/n_e studies presented in this article.

H_α emission diagnostics with line filters and photomultiplier tube (PMT) detectors are ideal tools to study plasma startup, fluctuations, and termination issues. In this article, H_α emission has been used to study breakdown physics on SSPX. H_α diagnostic study of the timing-dependent physics including particle confinement will be presented elsewhere.

II. TWO-CHORD CO_2 INTERFEROMETER

Through comparison of the phase difference between the laser beam that passes through the plasma (scene beam) and the laser beam that passes through the vacuum (reference beam), the line-integrated plasma density is obtained: $\int n_e dl = z m_e \varepsilon_0 \omega_0 c \int dl/\pi e^2$, where z is defined as the number of fringe shifts, which is related to the phase shift $\Delta\phi$ as $z=\Delta\phi/2\pi$, ω_0 is the laser frequency, ε_0 is the dielectric constant in the vacuum, m_e is the electron mass, c is the speed of light, and e is the electronic charge unit. For the CO_2 laser wavelength of 10.6 μm, and a typical spheromak line-averaged density of 10^{20} m^{-3} covering a 2 m pathlength, the phase shift is about two fringes.

The newly installed SSPX CO_2 interferometer uses the CTX experiment lasers, optics, and the optical table.[4] The layout of the CO_2 interferometer is shown in Fig. 1. Four significant issues needed to be addressed: vibration control, electronic noise reduction, phase demodulator modification, and laser temperature control.

It was critical to reduce the vibration during the CO_2 interferometer operation. Since the whole CO_2 system is on a wooden floor, there are interferences from natural building vibration and the shock due to capacitor bank discharge. The entire CO_2 interferometer system is isolated from the main SSPX vacuum chamber to reduce vibrations. All the optics and the lasers are mounted onto a 4 ft by 6 ft Newport Research Corporation (NRC) optical table. The optical table is supported on four NRC pneumatic legs, which are fixed to the main building floor beams. At the opposite side of the SSPX vacuum vessel, where the reflecting/return mirrors are located, there are two NRC pneumatic legs. The reflecting mirror mounting structure is coupled to the main optical table mounting structure using an aluminum beam yoke that go around the main SSPX vacuum vessel. Experimental data shows (see later) outstanding vibration isolation for at least 5–10 ms. The vibration noise level is of the order of 12 bit digitizer noise.

Double shielding capability of the signal lines was also important to the SSPX interferometer operation. To reduce electronic noise pickup, hard coax with SMA termination extends from each detector to the final signal-processing electronics, including an intermediate frequency (IF) ampli-

[a]Electronic mail: zwang@lanl.gov

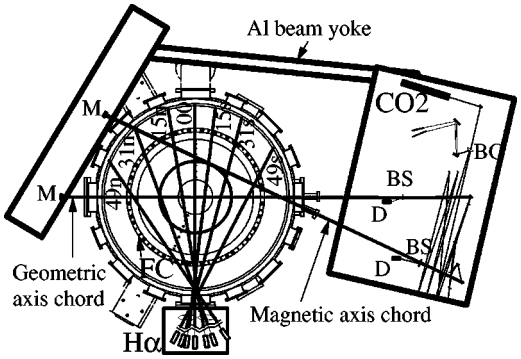

FIG. 1. The CO_2 interferometer and the H_α array diagnostics layout relative to the SSPX vacuum vessel. Seven midplane H_α line-of-sight and two CO_2 interferometer beam paths are shown. The Al beam structure couples the reflection side of the CO_2 interferometer to the main CO_2 optical table to effectively eliminate vibrations. M=mirror, BC=Bragg Cell, BS=beam splitter, D=CO_2 detector, and FC=flux conserver.

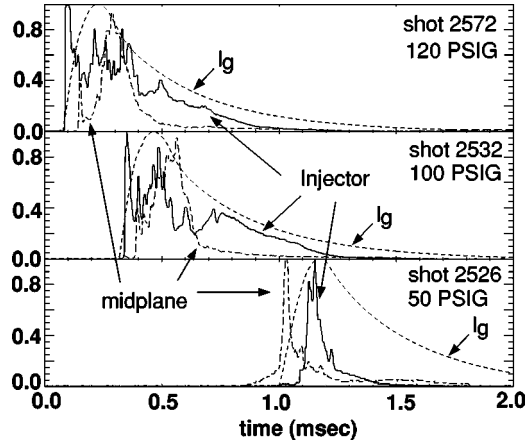

FIG. 2. Gas-breakdown delay time varies with the puffed gas amount. Comparisons are made for three shots at 50, 100, and 120 psi (gauge) hydrogen puff. For each shot, the solid curve is the injector H_α signal. Dashed curves are marked as midplane H_α signal and the total gun current I_g.

fier stage that automatically amplifies the interference signal from the detector and a phase demodulator stage that converts interference signals into phase and therefore the plasma density. Typical signal levels at the detector output are 5 mV, at IF amplifiers 1 V, and TTL at the phase demodulator output.

The phase demodulator was modified so that the electronic circuit can deal with an increased dynamic range that corresponds to 16 fringe counts. Densities that correspond to more than 16 fringes can be retrieved using postprocessing IDL routines. (In comparison, the original circuit had a dynamic range of 8 fringe counts, and could not deal with the signals greater than this range.) Basically, XOR gates (DM74S86N type) in the circuit were replaced by reset/set latches using fast NAND gates (SN74S00 type). The total delay of the modified circuit was on the order of 20 ns, while the phase data was digitized at 1 MHz using Model TR612 Joerger digitizers. Each Joerger digitizer channel also has a 12 bit dynamic range and enough memory to hold 8 kbytes of data for each density chord in every single shot.

Another important factor in the successful operation of the CO_2 interferometer was reducing the tendency of the laser cavity to mode hop by carefully controlling the cavity temperature. The 7 W Laakmann CO_2 laser is driven by a 40 MHz radio frequency (rf) amplifier which is dc powered at 10 A and 20 V, but operated in a pulsed ($\sim$10 ms duration) mode. The laser temperature determines the laser cavity length and therefore the lasing wavelength. The P20 line is the one that the interferometer optics layout and the Bragg cell are aligned for. Only when the laser temperature is accurate within 0.1 K of the set temperature, could continuous and consistent laser power at P20 line for a 10 ms laser pulse duration be secured.

Two CO_2 chords are presently operational. One chord goes through the theoretical magnetic axis of the spheromak with an effective path length of 1.53 m. The other chord goes through the geometrical axis of the spheromak, with a total path length of 2.00 m. All the optical window for the CO_2 chords are 1 in. diameter ZnSe plates. ZnSe plates replace the salt (NaCl or KCl) windows as previously used on CTX. ZnSe plates are superior to the salt, because of their better vacuum compatibility and freedom from water condensation. Both the magnetic and geometric axis chords have an incident angle a few degrees off the ZnSe surface normal. The entrance and the exit window of the magnetic axis chord are reflection compensated with quarter wavelength interference coating, so the reflection loss is reduced to minimum. The geometrical-axis windows are not compensated. The reflection loss causes a reduction of its signal to about one fifth of the magnetic-axis signal.

III. H_α ARRAY

The location of the H_α array relative to the SSPX vacuum vessel is shown in Fig. 1. The size of the detector array and its shield box is 5 in. by 10 in. by 10 in. The heart of the diagnostic is a Hamamatsu HC120-05 compact PMT detector assembly. This assembly combines a 1/2 in., side-on PMT (R3823 type) with a high voltage power supply, voltage divider, and buffer amplifier to measure the weakest light signals. Each individual detector channel is about 1 in. by 1 in. cross section, and 5 in. long. A dc voltage of 0 to +5 V is needed to power the PMTs. The dc voltage can be remotely controlled through CAMAC. This assembly has a spectral range of 185–900 nm, an amplifier feedback resistor of 100 kΩ, a gain of 60 V/nW at 650 nm, and a bandwidth of 200 kHz.

To measure H_α signals, filters of 10 nm bandwidths at 656.2 nm are inserted before the entrance slit to the PMTs. The transmission of the filters at the H_α wavelength is usually 65%. All H_α channels are cross calibrated relative to each other using a continuum light source. All channels use 600 μm diameter optical fiber of proper length to transmit light from the vacuum windows to the detector assembly. For SSPX, seven channels monitor the H_α light in the midplane at angles of $-49°$, $-31°$, $-15°$, 0°, 15°, 31°, and 49° relative to the channel that goes through the geometric axis of the vacuum chamber (0° channel). These chords are labeled as 49*n*, 31*n*, 15*n*, 00, 15*s*, 31*s*, and 49*s* in Fig. 2. Optical fibers are positioned at the focal plane of two similar-focal-length lenses at the machine end, pointing at

angles mentioned above. An eighth channel (not shown in Fig. 2) monitors light from the coaxial plasma injector. The H_α injector monitor is mounted on the gun wall at an angle of 45° with respect to the symmetric axis of the gun cylinder, viewing only inside the injector.

Total plasma current and its distribution within a spheromak were indirectly measured by the magnetic probes on the gun wall and flux conserver wall. An axisymmetric magnetohydrodynamic (MHD) code CORSICA[5] was used to reconstruct the total plasma current. Other SSPX diagnostics are describe elsewhere.[6]

IV. RESULTS AND DISCUSSION

Figure 2 shows the H_α light emission (injector and one midplane chord) for three different gas puff amounts, 50 pound per square inch gauge [psi (gauge)], 100, and 120 psi (gauge), under similar conditions. [1 psi (gauge)$\equiv$1+ 14.7 psi]. Generally, signals from H_α channels have a lot of temporal structure. Spatially, the south port view does not show symmetry with its north port counterpart. Since H_α light is mostly from edge plasma, this indicates a break in symmetry at the spheromak edge, and probably complicated boundary physics. However, the startup timing of all the midplane chord signals are well synchronized, so we need only look at one midplane chord for the breakdown physics described here.

It took significantly longer to break down at 50 psi (gauge) than at 120 psi (gauge). In addition, H_α light appeared earlier in the midplane than in the injector for 50 psi (gauge), while the opposite was true for the 120 psi (gauge) case.

Using the Paschen characteristics of hydrogen gas breakdown in the gun,[7,8] it was estimated that the minimum breakdown voltage corresponds to a plenum gas fill of $\sim$108 psi (gauge). This number is consistent with Fig. 2. 120 psi (gauge) is greater than this number, so the breakdown took place within the gun injector. Once the gas filled the gap between the electrodes ($\sim$100 μs). Therefore, injector light appeared earlier than the midplane. For the 50 psi (gauge) case, the breakdown happened only when the gas traveled down the gun electrodes into the flux conserver; there, a much longer path length was possible, and the Paschen breakdown criterion was met. Therefore, the midplane H_α light comes up first, with a much longer delay in breakdown than 120 psi (gauge) case.

A typical SSPX shot is shown in Fig. 3. The last two traces from the top correspond to the plasma density. The average noise corresponds to a density uncertainty of 2×10^{18} m^{-3}. Density traces are completely free of vibrations for more than 6 ms, much longer than the shot duration of $\sim$2 ms. There is $\sim$ 70 μs with no density data because the main formation bank firing causes noise pickup in the phase demodulation circuit. The ratio of line-averaged density of the geometric axis chord to magnetic axis chord was essentially unity throughout the shot, indicating a relatively flat density profile. We calculate a J/n_e parameter based then on a calculated average J and our line-averaged n_e. An interesting dip in density at time 1.38 ms with no corresponding

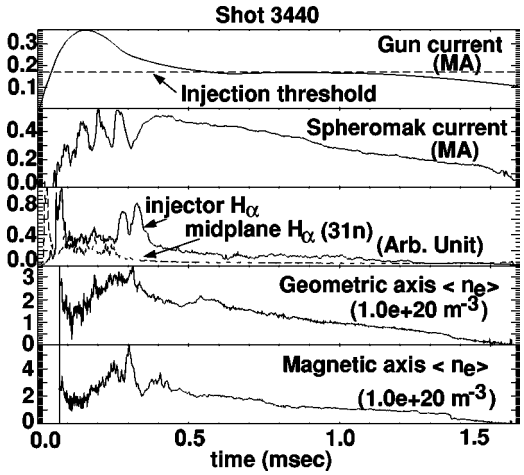

FIG. 3. An example shot. $t=0$ was when the FB was fired. FB was charged to 7 kV. H_2 gas of 120 psi (gauge) pressure in eight plenums (total volume of 1.5 cm^3) was puffed into the gun 650 μs earlier than the FB discharge. The 1.3 kV SB was discharged at 100 μs after the FB. Initial gun flux was 15 mWb.

magnetic signature might be related to pressure driven instability.[9] Corresponding to the dip, the J/n_e parameter jumped from $\sim1.0\times10^{-14}$ A m before the event to values greater than 2.0×10^{-14} A m and increasing afterwards. Other relevant data about the shots are: the top plot showing the gun current with the minimum current threshold for helicity injection $I_{\rm th}=\lambda_{\rm th}\varphi_g/\mu_0$;[8] the second plot showing CORSICA fit of spheromak current, which corresponds to 1.6 kG peak magnetic field. To obtain the averaged spheromak current density for J/n_e parameter, simply divide the J fit to the total area of the poloidal spheromak area, 0.255 m^2 in our case. The third plot showing both the injector and the midplane $31n$ H_α chords.

Initial gas puff amount, bank-firing timing, wall sputtering can affect the spheromak plasma density. Baking, Ti ball gettering of the flux conserver, glow discharge cleaning, He-gas purge were used to reduce the wall effects. Experimental data on the density in SSPX so far can be summarized as follows: The density does not correlate with the gas puff amount. The density increased when the formation bank (FB) or the sustainment bank (SB) voltages were increased. Flux conserver gettering did not show any impact on the density under similar experimental conditions. (Gettering did show significant impact on other plasma parameters, such as total radiated power measured by bolometers, which are not covered in this discussion.) When other experimental conditions were fixed, the density n_e scaled with SB voltage $V_{\rm SB}$ roughly as $n_e\propto V_{\rm SB}^2$, see Fig. 4. The experimental data show that the density from the gun walls is a main particle source, in particular, during the sustainment phase. It is estimated that one monolayer of the surface particles (4.6 m^2 surface area) would be equivalent to 60 psi (gauge) of the 1.5 cm^3 plenum H_2 fill.

The total plasma current depends on the helicity injected and plasma resistivity.[10] Under similar conditions, increased formation bank energy did not increase the spheromak current in proportion. As expected,[8] there is an optimal gun flux φ_g (about 20 mWb) to maximize magnetic helicity injected

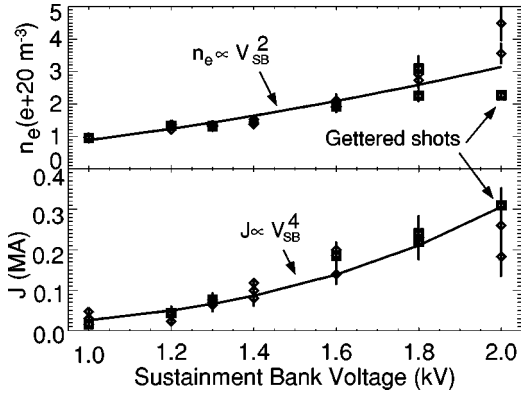

FIG. 4. Line average electron density and spheromak current variation (averaged between 1.2 and 1.4 ms) with sustainment bank voltage, when other parameters are fixed. Gun flux was 15 mWb, FB voltage 5 kV, H_2 gas, and 140 psi (gauge) puff pressure.

$2V_g\varphi_g$, above which the gun voltage V_g reduces too much. Late in time, total spheromak current J scaled with V_{SB} roughly as $J \propto V_{SB}^4$, see Fig. 4. Combining J and n_e data, we find that J/n_e rarely exceeds 2.0×10^{-14} A m. J/n_e variations with formation bank energy were mainly due to variations of the plasma density, not plasma current. Therefore, J/n_e gets worse at high FB energies. Late in time, J/n_e variation with SB energy (when other experimental parameters were fixed.) can be roughly fitted by $J/n_e \propto V_{SB}^2$ for SB voltages between 1.0 and 2.0 kV.

V. CONCLUSIONS

A two-chord CO_2 interferometer and an eight-channel H_α array are successfully implemented for the new SSPX. Techniques are described to reduce the vibration and electronic noise pickup in the density measurements. New phase analysis electronics and precise-laser-temperature control were also critical for the CO_2 interferometer operation. The density data indicated that the interferometer is free of vibration for more than 6 ms, much longer than a typical shot duration of 2–3 ms. The noise level of the density signals is equivalent to $\sim 2\times10^{18}$ m^{-3}. Such a noise level usually corresponds to a signal-to-noise ratio of 50. Typical plasma density is a few times 10^{20} m^{-3}. Density measurement coupling with CORSICA modeling and magnetic probe measurement yields the (spatially averaged) J/n_e parameter. Typically, J/n_e is less than 2×10^{-14} A m, which is at the low end of where we would like to control this parameter. Spheromak operation with larger SB energy and varied timing of SB firing relative to FB firing is highly desirable. Ti ball gettering of the plasma gun surface might be a useful density control technique.

ACKNOWLEDGMENTS

The authors thank F. J. Wysocki for many stimulating discussions. This work is supported by U.S. DOE Contract No. W-7405-EN6-36.

[1] E. Bickford Hooper, J. H. Hammer, C. W. Barnes, J. C. Fernandez, and F. J. Wysocki, Fusion Technol. **29**, 191 (1996).
[2] T. K. Fowler, Fusion Technol. **29**, 206 (1996).
[3] E. B. Hooper and T. K. Fowler, Fusion Technol. **30**, 1390 (1996).
[4] E. W. Newman, C. J. Buchenauer, and H. W. Hoida, Rev. Sci. Instrum. **57**, 1992 (1986).
[5] E. B. Hooper, L. D. Pearlstein, and R. H. Bulmer, Nucl. Fusion **39**, 863 (1999).
[6] H. McLean *et al.*, Rev. Sci. Instrum., these proceedings.
[7] J. C. Fernandez *et al.*, Nucl. Fusion **28**, 1555 (1988).
[8] C. W. Barnes, T. R. Jarboe, G. J. Marklin, S. O. Knox, and I. Henins, Phys. Fluids B **2**, 1871 (1990).
[9] F. J. Wysocki, J. C. Fernandez, I. Henins, T. R. Jarboe, and G. J. Marklin, Phys. Rev. Lett. **61**, 2457 (1988).
[10] C. W. Barnes, J. C. Fernandez, I. Henins, H. W. Hoida, T. R. Jarboe, S. O. Knox, G. J. Marklin, and K. F. McKenna, Phys. Fluids **29**, 3415 (1986).